IEEE Access
Multidisciplinary | Rapid Review | Open Access Journal

Received 9 October 2023, accepted 2 November 2023, date of publication 6 November 2023, date of current version 9 November 2023.

Digital Object Identifier 10.1109/ACCESS.2023.3330440

RESEARCH ARTICLE

Nonlinear Observer-Based Controller Design for VSC-Based HVDC Transmission Systems Under Uncertainties

ILYASS EL MAYSSE[1], (Student Member, IEEE), ABDELMOUNIME EL MAGRI[1], AZIZ WATIL[1], ABDULAZIZ ALKUHAYLI[2], MOHAMMED KISSAOUI[1], RACHID LAJOUAD[1], FOUAD GIRI[3], AND MOHAMED METWALLY MAHMOUD[4]

[1]Laboratory of Electrical Engineering and Intelligent Systems, ENSET Mohammedia, Hassan II University of Casablanca, Mohammedia 28810, Morocco
[2]Department of Electrical Engineering, College of Engineering, King Saud University, Riyadh 11421, Saudi Arabia
[3]Caen Automation Laboratory (LAC), University of Caen Normandie, 14118 Caen, France
[4]Department of Electrical Engineering, Faculty of Energy Engineering, Aswan University, Aswan 81528, Egypt

Corresponding author: Ilyass El Maysse (ilyass.elmyasse-etu@etu.univh2c.ma)

This work was supported by King Saud University, Riyadh, Saudi Arabia, through the Researchers Supporting Project under Grant RSP2023R258.

ABSTRACT This paper addresses the problem of output feedback control for high voltage direct current (HVDC) systems based on voltage source converters (VSC). Specifically, the system under study consists of two power grids and two VSC stations connected via a long HVDC cable. The primary goal of this paper is to propose a different approach for the online estimation of the grid voltage placed at a great distance from the control unit which is considered generally known, moreover the proposed technique aims to online estimation of the grid pulsation and the HVDC cable states, generally considered available. A nonlinear observer is intended to address these concerns. Only the line current measurements are used to estimate all state variables. Furthermore, utilizing the estimation offered by the proposed observer, an output feedback control strategy is formulated, using the backstepping design technique, to meet the three control objectives: 1) tight output voltage regulation of the HVDC cable; 2) ensuring a perfect power quality at both sides of the HVDC system; 3) regulation of the active power at the inverter station. The high effectiveness of the proposed output feedback controller's performance is highlighted via a semi-experimental platform that includes a Processor In the Loop (PIL) on the embedded board eZdsp. Extra numerical simulations show that The proposed output feedback performance enjoys additional robustness properties and meets all control objectives.

INDEX TERMS HVDC transmission, backstepping control, nonlinear observer, high gain observer, power converter control, PFC, VSC-HVDC, HVDC cable.

I. INTRODUCTION

High-voltage direct current (HV DC) transmission systems are becoming progressively important in power systems around the world that are marked by a growing demand for electricity and the need to reduce gas emissions from fossil fuel sources [1], [2]. HVDC technology is the most efficient way of transporting a significant amount of electricity over great distances, as well as assisting in the integration of renewable energy sources into the grid, interconnection of asynchronous grids, and the stabilization of three-phase systems [3], [4].

In order to use DC, there are two technologies available for converting high voltage AC power to DC power: the traditional Line Commutated Converter (LCC) and the Voltage Source Converter (VSC). Compared to standard LCC schemes, VSC offers a number of technological advantages because it generates an AC waveform that allows the system to control reactive power independently of active power regulation [5]. Therefore, researchers are actively studying

The associate editor coordinating the review of this manuscript and approving it for publication was Sonia F. Pinto.

control techniques to ensure the robust operation of VSC HVDC systems under a wide range of operating conditions and disturbances.

Numerous research on modeling and controlling the VSC HVDC systems using traditional proportional-integral (PI) control have already been performed [6], [7]. However, the performance of these controllers is highly dependent on their design parameters, which are adjusted by the one-point linearization of the system. This implies that if the system's operating conditions change according to the point linearization, the system's performance may decrease. To deal with this issue, nonlinear controls have been proposed such as backstepping control [8], adaptive control [9], feedback linearization controller associated with gain scheduling [10], fuzzy control, and anti-windup action [11], optimal data-driven control strategy [12], model predictive control strategy [13], [14], sliding mode control [15], passivity-based control design [16], [17]. The point is that all the previous studies all designed in $d-q$ reference frame. Their performances strongly depend on current decoupling, Such a decoupling is usually accomplished with a phase-locked loop (PLL). whose dynamics can negatively affect the operation of the system. Indeed, PLL dynamics include time delays, nonlinearities, and interaction with the grid impedance. All these factors are likely to cause a reduction in the performance of the system [18], [19], [20]. To get around the negative impact generated by the PLL dynamics, a nonlinear observer is proposed in this paper that estimates the pulsation and electrical position.

In the past few decades, several nonlinear observer-based controllers have been developed to estimate the unavailable system states and mitigate external perturbations and system uncertainties. These controllers proved to be able to enhance the dynamic performance of renewable energy sources [21], [22] as well as HVDC electric transport networks [23], [24]. The authors in [23] used an ESO called perturbation observer-based sliding-mode control to predict the combinatorial effect of nonlinearities and parameter uncertainties in VSC-HVDC systems in [24], a perturbation observer-based nonlinear control scheme was proposed, that includes a feedback linearization control law and a high gain observer; the controller also proved to be useful in estimating model uncertainties. The point is that the mentioned works did not take into account the dynamic characteristics of the HVDC cable and therefore cannot ensure the robust operation of the VSC HVDC system. Furthermore, the grid voltage, the angular frequency, and electrical position are considered known and available, as well as the states of the DC side and the inverter current, which are considered accessible for measurement.

In this work, we develop an advanced output-feedback controller for a two-terminal VSC-HVDC electric power transmission system, in order to enhance its overall performance, reliability, and efficiency. First, we establish the system model and transform it to a canonical form that is based upon to design a high-gain state observer in the $\alpha\beta$-coordinates frame. The observer provides online estimation of two important variables, i.e., the power grid frequency, voltage at the primary of the transformer as well as the inverter current. Furthermore, the regulation of the output voltage of the HVDC cable which is the prime control objective is also considered as inaccessible to measurement. Only line currents are assumed to be measured. Then, based on the online estimation provided by the observer, an output feedback control is developed using the backstepping technique with the Lyapunov approach to ensure stability and guarantee robustness to disturbance.

The rest of the paper is structured as follows: The VSC-HVDC transmission system under study is presented and modeled in section II. Section III is devoted to the state feedback design and analysis using backstepping and Lyapunov approaches. The nonlinear observer design and its stability are analyzed in section IV. Section V includes numerical simulations which illustrate the output feedback controller's performance. Section VI brings the paper to a close.

II. MATHEMATICAL MODEL OF HVDC SYSTEMS BASED ON VSC

Figure 1 presents the circuit illustration of a two-terminal HVDC transmission system based on VSC. Terminal 1 consists of AC grid 1 which is connected to VSC1 using a serial transformer 1 and phase reactor (R_1, L_1). Similarly, terminal 2 consists of AC grid 2 connected to converter station VSC2 via a serial transformer 2 and phase reactor (R_2, L_2).

Remark 1: When power flow is from terminal 1 (terminal 2) to terminal 2 (terminal 1) converter VSC1 (VSC2) will have DC voltage control and reactive power control, and converter VSC2 (VSC1) will have active and reactive power control. In this research, for analysis purposes, one considers power flow from terminal 1 to terminal 2.

A. THE CONVERTER STATION MODEL

The converter stations are linked to a three-phase network, as illustrated in Figure 1. In the rotating $d-q$ reference frame, the model of the rectifier station (VSC 1) is expressed as follows [21], [25]:

$$\begin{aligned}\frac{di_{d_1}}{dt} &= -\frac{R_1}{L_1}i_{d_1} + \omega_1 i_{q_1} + \frac{e_{d_1}}{L_1} - \frac{u_{d_1}}{L_1}\\ \frac{di_{q_1}}{dt} &= -\frac{R_1}{L_1}i_{q_1} - \omega_1 i_{d_1} + \frac{e_{q_1}}{L_1} - \frac{u_{q_1}}{L_1}\end{aligned} \tag{1}$$

Similarly, The dynamics model of the inverter station (VSC 2) can be represented in the $dq-$coordinates as follows [26]:

$$\begin{aligned}\frac{di_{d_2}}{dt} &= -\frac{R_2}{L_2}i_{d_2} + \omega_2 i_{q_2} - \frac{e_{d_2}}{L_2} + \frac{u_{d_2}}{L_2}\\ \frac{di_{q_2}}{dt} &= -\frac{R_2}{L_2}i_{q_2} - \omega_2 i_{q_2} - \frac{e_{q_2}}{L_2} + \frac{u_{q_2}}{L_2}\end{aligned} \tag{2}$$

where (u_d, u_q), (e_d, e_q), and (i_d, i_q) represent the control inputs of the converter stations, the voltages and currents of the AC grids in $dq-$coordinates, respectively. And ω is the networks pulsation.

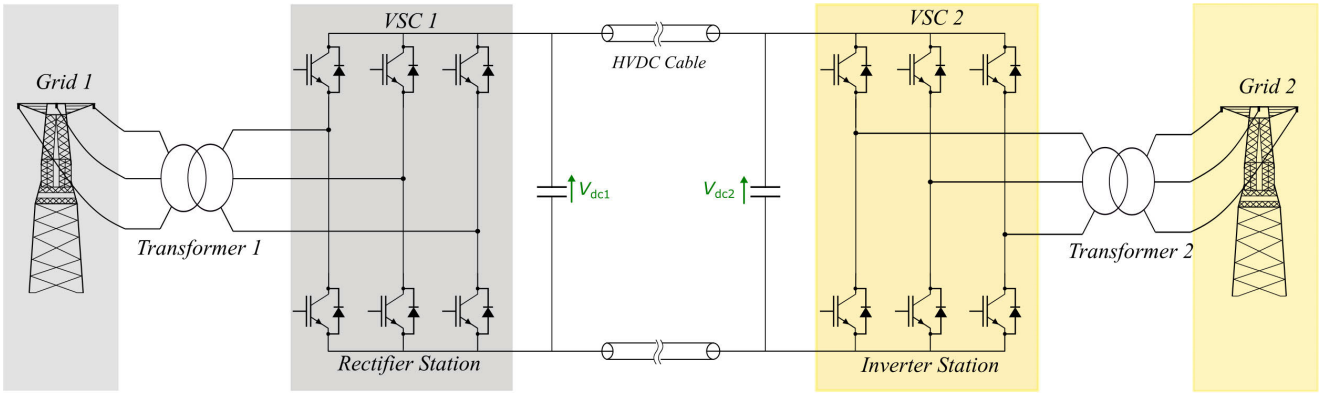

FIGURE 1. Topology of VSC-based HVDC transmission system.

B. THE DC SIDE MODEL

The DC cable can be conceptualized as a series of linked sections. There are different kinds and configurations of these DC cable sections, specifically the "T" type section and the "π" type section. In this case, we are specifically examining the structure of the π-section as depicted in Figure 2. This section was chosen because of its simplicity, which allows for an analytical derivation while still representing the resonance of a DC transmission line [27]. This structure is characterized by:

- Resistance R_c: it models the Joule effect losses in the DC cable.
- Inductance L_c: It embodies the inherent magnetic characteristics of the wire and the mutual magnetic effect between the two wires of the cable.
- Capacitance C_c: It represents the electrostatic characteristics of a dielectric material, with its value contingent on the material's physical and geometrical properties.

The HVDC cable equivalent electrical model is given in figure 2, the model of the DC side is described by [28]:

$$\begin{aligned}\frac{dV_{dc1}}{dt} &= \frac{e_{d_1} i_{d_1}}{C_{eq} V_{dc_1}} - \frac{i_c}{C_{eq}} \\ \frac{dV_{dc2}}{dt} &= \frac{i_c}{C_{eq}} - \frac{i_{inv}}{C_{eq}} \\ \frac{di_c}{dt} &= -\frac{R_c}{L_c} i_c + \frac{V_{dc_1} - V_{dc_2}}{L_c}\end{aligned} \tag{3}$$

with $C_{eq} = C + C_c$, and (V_{dc_1}, V_{dc_2}) respectively, are the input and output voltages of the HVDC cable, and i_c is the cable current.

Remark 2: According to the literature [29], a pi-section model is recommended for medium transmission lines 80 to 250km long. This model is suitable for the length of the line used in our study.

C. THE AVERAGE MODEL OF THE VSC-HVDC SYSTEM.

To deal with the binary character of the input signal, controller design is typically carried out using averaged models.

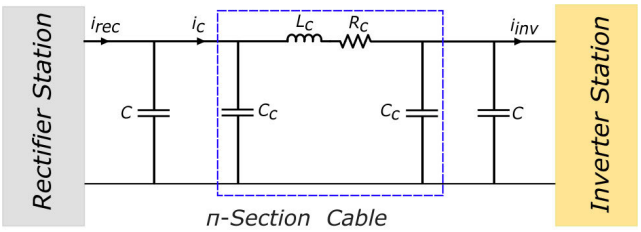

FIGURE 2. Structure of the HVDC cable.

To this end, the averaged versions of the instantaneous variables $[V_{dc_2}, i_c, V_{dc_1}, i_{d_1}, i_{q_1}, i_{d_2}, i_{q_2}]$ are denoted by $[\bar{x}_1, \bar{x}_2, \bar{x}_3, \bar{x}_4, \bar{x}_5, \bar{x}_6, \bar{x}_7]$. Then, the state space representation of the global system rewrites as follows:

$$\dot{\bar{x}}_1 = \frac{\bar{x}_2}{C_{eq}} - \frac{i_{inv}}{C_{eq}} \tag{4.1}$$

$$\dot{\bar{x}}_2 = -\frac{R_c}{L_c}\bar{x}_2 - \frac{\bar{x}_1}{L_c} + \frac{\bar{x}_3}{L_c} \tag{4.2}$$

$$\dot{\bar{x}}_3 = \frac{e_{d_1}}{C_{eq}\bar{x}_3}\bar{x}_4 - \frac{\bar{x}_2}{C_{eq}} \tag{4.3}$$

$$\dot{\bar{x}}_4 = -\frac{R_1}{L_1}\bar{x}_4 + \omega\bar{x}_5 - \frac{u_{d_1}}{L_1} + \frac{e_{d_1}}{L_1} \tag{4.4}$$

$$\dot{\bar{x}}_5 = -\frac{R_1}{L_1}\bar{x}_5 - \omega\bar{x}_4 - \frac{u_{q_1}}{L_1} \tag{4.5}$$

$$\dot{\bar{x}}_6 = -\frac{R_2}{L_2}\bar{x}_6 + \omega\bar{x}_7 + \frac{u_{d_2}}{L_2} - \frac{e_{d_2}}{L_2} \tag{4.6}$$

$$\dot{\bar{x}}_7 = -\frac{R_2}{L_2}\bar{x}_7 - \omega\bar{x}_6 + \frac{u_{q_2}}{L_2} \tag{4.7}$$

III. STATE FEEDBACK NONLINEAR CONTROL DESIGN

The goal of this section is to build a nonlinear controller for a two-terminal VSC-HVDC transmission system that meets the following control objectives simultaneously:

- Regulation of the output voltage DC cable, through the rectifier station, enforcing it to track a given reference signal V^*_{dc2}.
- Power factor correction, i.e., the grid currents must be sinusoidal and in phase with the grid voltages.

- Regulation of the active power P_2 at the inverter station ($VSC2$).

For this purpose, based on the proceeding of works [25], [30], the control design will be carried out using the backstepping technique.

A. RECTIFIER CONTROL DESIGN

The rectifier station operates in the DC voltage control mode, with the output DC cable voltage V_{dc2} and the reactive power Q_1 as the controlled variables.

1) DC VOLTAGE LOOP

The HVDC cable output voltage must converge to a given reference voltage. Based on subsystem (4.1)-(4.4), the design of the backstepping control is completed in four steps.

a: STEP 1

Let us introduce the HVDC voltage tracking error: $e_1 = \bar{x}_1 - x_1^*$. in view of (4.1), the dynamic of the above error is obtained as follows:

$$\dot{e}_1 = \frac{1}{C_{eq}}\bar{x}_2 - \frac{1}{C_{eq}}i_{inv} \tag{5}$$

in (5), the quantity $\frac{1}{C_{eq}}\bar{x}_2 = \alpha_1$ stand as a virtual control variable. Then e_1 will vanish if the stabilizing function α_1 is defined by

$$\alpha_1 = -c_1 e_1 + \frac{1}{C_{eq}}i_{inv} \tag{6}$$

with $c_1 > 0$. Indeed, this choice implies that $\dot{e}_1 = -c_1 e_1$ which ensures asymptotic stability of (4.1) with respect to the Lyapunov function: $V_1 = 0.5\, e_1^2$. Actually, then one gets $\dot{V}_1 = -c_1 e_1^2$ which is negative definite with respect to $\dot{e}_1$.

As α_1 is not the actual control input, we introduce the following new tracking error: $e_2 = \frac{1}{C_{eq}}\bar{x}_2 - \alpha_1$. Combining equations (5) and (6), we find:

$$\dot{e}_1 = e_2 - c_1 e_1 \tag{7}$$

b: STEP 2

Stabilization of the system error (e_1, e_2).

Now, the purpose is to enforce the errors (e_1, e_2) to vanish. The derivative of e_2 is:

$$\dot{e}_2 = -\frac{R_c}{C_{eq}L_c}\bar{x}_2 + \frac{1}{C_{eq}L_c}\bar{x}_3 - \frac{1}{C_{eq}L_c}\bar{x}_1 - \dot{\alpha}_1 \tag{8}$$

The quantity $\frac{1}{C_{eq}L_c}\bar{x}_3 = \alpha_2$, in (8), stands as a new virtual control. Following the backstepping design technique, the errors (e_1, e_2) will be asymptotically vanishingh if the stabilizing function α_2 is defined as follows:

$$\alpha_2 = -e_1 - c_2 e_2 + \frac{R_c}{C_{eq}L_c}\bar{x}_2 + \frac{1}{C_{eq}L_c}\bar{x}_1 + \dot{\alpha}_1 \tag{9}$$

As α_2 is not the control input, we introduce the new tracking error: $e_3 = \frac{1}{C_{eq}L_c}\bar{x}_3 - \alpha_2$. Then, (8) can be rewrite as follows:

$$e_2 = -c_2 e_2 + e_3 \tag{10}$$

c: STEP 3

Stabilization of the system error (e_1, e_2, e_3).

In this step, the aim is to make the error system (e_1, e_2, e_3) asymptotically stable. Using equation(4.3), the derivative of e_3 is given by:

$$\dot{e}_3 = \frac{e_{d_1}}{L_c C_{eq} C_{eq}}\frac{\bar{x}_4}{\bar{x}_3} - \frac{1}{L_c C_{eq} C_{eq}}\bar{x}_2 - \dot{\alpha}_2 \tag{11}$$

To find a stabilizing control law for (11), similar steps as above. It turns out that the error system (e_1, e_2, e_3) asymptotically stable if α_3 is defined as follows:

$$\alpha_3 = -e_2 - c_3 e_3 + \frac{1}{L_c C_{eq} C_{eq}}\bar{x}_2 + \dot{\alpha}_2 \tag{12}$$

As α_3 is not the actual control input, we introduce the new tracking error: $e_4 = \frac{1}{L_c C_{eq} C_{eq}}\bar{x}_4 - \alpha_3$. Combining (11) and (12), equation (11) becomes:

$$e_3 = -c_3 e_3 + e_4 \tag{13}$$

d: STEP 4

Stabilization of the subsytem error (e_1, e_2, e_3, e_4). It is readily checked that the time derivative of e_4 is:

$$\dot{e}_4 = \frac{1}{L_1 L_c C_{eq} C_{eq}}\left(-R_1\bar{x}_4 + L_1\omega_1\bar{x}_5 - u_{d_1} + e_{d_1}\right) - \dot{\alpha}_3 \tag{14}$$

Now, the objective is to make the error system (e_1, e_2, e_3, e_4) asymptotically stable. A sufficient condition is to let the derivative of e_4 be defined as follows, for some $c_4 > 0$:

$$\dot{e}_4 = -e_3 - c_4 e_4 \tag{15}$$

Using (14) and (15), one gets the following control law:

$$u_{d_1} = \frac{L_1}{\beta}\left[e_3 + c_4 e_4 + \beta(-\frac{R_1}{L_1}\bar{x}_6 + \omega_1\bar{x}_7 + \frac{e_{d_1}}{L_1}) - \dot{\alpha}_3\right] \tag{16}$$

2) REACTIVE POWER LOOP (PFC OBJECTIVE)

In this part, we seek to make the reactive power Q_1 regulated to its reference signal Q_1^*. Recall that the reactive power is $Q_1 = e_{d_1} i_{q_1}$. Introducing, the reactive power tracking error: $e_5 = e_{d_1}\bar{x}_5 - Q_1^*$. It follows, using (4.5):

$$\dot{e}_5 = e_{d_1}\left[-\frac{R_1}{L_1}\bar{x}_5 - \omega_1\bar{x}_4 - \frac{1}{L_1}u_{q_1}\right] \tag{17}$$

We aim at enforcing the error e_5 to be asymptotically vanishing. To this end, we consider the Lyapunov function candidate $V_5 = 0.5 e_5^2$. Its time derivative $\dot{V}_5 = e_5\dot{e}_5$ can be

rendered negative definite function if the dynamics of e_5 is selected as follows, for some $c_5 > 0$:

$$\dot{e}_5 = -c_5 e_5 \tag{18}$$

Comparing (18) with (17), we obtain the following input control law u_{q_1}:

$$u_{q_1} = \frac{1}{L_1}\left[\frac{c_5 e_5}{e_{d_1}} - \omega_1 \bar{x}_4 - \frac{R_1}{L_1}\bar{x}_5\right] \tag{19}$$

Proposition 1: Take into consideration the closed-loop system that encompasses the AC/DC converter-DC cable, described by equations (4.1)-(4.7), along with the nonlinear control laws (16) and (19). Under these conditions, the behavior of the error system within the closed-loop is governed by the ensuing equation:

$$\begin{pmatrix}\dot{e}_1\\ \dot{e}_2\\ \dot{e}_3\\ \dot{e}_4\\ \dot{e}_5\end{pmatrix} = B\begin{pmatrix}e_1\\ e_2\\ e_3\\ e_4\\ e_5\end{pmatrix} \text{ with } B = \begin{pmatrix}-c_1 & 1 & 0 & 0 & 0\\ -1 & -c_2 & 1 & 0 & 0\\ 0 & -1 & -c_3 & 1 & 1\\ 0 & 0 & -1 & -c_4 & 0\\ 0 & 0 & 0 & -1 & -c_5\end{pmatrix} \tag{20}$$

Furthermore, the system error (20) is asymptotically stable. Accordingly, the error vector $(e_1, e_2, e_3, e_4, e_5)$ is exponentially vanishing, whatever the initial condition.

Proof: Equation (20) is immediately obtained from (7), (10), (13), (15) and (18). The state matrix B is clearly Hurwitz, implying that the linear closed-loop system (20) is globally asymptotically stable.

B. INVERTER CONTROL DESIGN

The inverter station is designated for active and reactive power control. The involved DC voltage has to be regulated to a constant value. As for the active power $P_2 = e_{d_2}\, i_{d_2}$ and reactive power $Q_2 = e_{d_2}\, i_{q_2}$, they are separately controlled by acting on the direct current i_{d_2} and the quadrature current i_{q_2}, respectively.

1) ACTIVE POWER LOOP

In this subsection, the purpose is to enforce the direct current x_6 to track a given reference signal $x_6^* = \dfrac{P_2^*}{e_{d_2}}$. To this end, introduce the direct current tracking error $e_6 = \bar{x}_6 - x_6^*$. From (4.6), it follows:

$$\dot{e}_6 = -\frac{R_2}{L_2}\bar{x}_2 + \omega_2 \bar{x}_7 + \frac{u_{d_2}}{L_2} - \frac{e_{d_2}}{L_2} - \dot{x}_6^* \tag{21}$$

To get a stabilizing control law for (21), we consider the Lyapunov function candidate $V_6 = 0.5\, e_6^2$. Its time derivative $\dot{V}_6 = e_6 \dot{e}_6$ is made negative definite function by letting $\dot{e}_6$ be as follows for some $c_6 > 0$:

$$\dot{e}_6 = -c_6 e_6 \tag{22}$$

Comparing (21) and (22), following control law:

$$u_{d_2} = L_2\left[-c_6 e_6 + \frac{R_2}{L_2}\bar{x}_6 - \omega_2 \bar{x}_7 + \frac{e_{d_2}}{L_2} + \dot{x}_6^*\right] \tag{23}$$

2) REACTIVE POWER LOOP

Following similar steps III-A2, the control law u_{q_2} is obtained as follows:

$$u_{q_2} = L_2\left[-\frac{c_7 e_7}{e_{d_2}} + \frac{R_2}{L_2}\bar{x}_7 + \omega_2 \bar{x}_6\right] \tag{24}$$

Proposition 2: Consider the subsystem (4.6)-(4.7) together with the control laws (23) and (24) with c_6 and c_7 being arbitrary positive constant. Then, one has the following properties:

1) The closed-loop error system with state vector (e_6, e_7) undergoes the following equations:

$$\begin{aligned}\dot{e}_6 &= -c_6 e_6\\ \dot{e}_7 &= -c_7 e_7\end{aligned} \tag{25}$$

2) This linear system is globally asymptotically stable with respect to the candidate Lyapunov function $V(e) = 0.5e_6 + 0.5e_7$. Therefore, for any positive design parameters c_6 and c_6, the system error (e_6, e_7) vanishes exponentially, whatever the initial conditions.

IV. OUTPUT FEEDBACK CONTROL DESIGN

The purpose of this section is to design a nonlinear observer and use it to design an output feedback controller.

A. MODELING OF THE VSC-HVDC IN THE $\alpha\beta$-FRAME

Because the grid pulsation and voltage are not assumed to be available to measurement, the VSC-HVDC system model is now considered in the $\alpha\beta-$coordinates which is more appropriate for observer design (while the $dq-$coordinates are commonly employed in control design due to their simplicity). Inspired by [21] and [22] the complete model expressed in $\alpha\beta-$coordinates is splitted in two subsystems, denoted $\mathbb{S}_1$ and $\mathbb{S}_2$:

$$\mathbb{S}_1 : \begin{cases}\dot{X}_1 = f_1(x(t), u(t)) + \delta_1(t)\\ y_1 = C_1 X_1\end{cases} \tag{26}$$

$$\mathbb{S}_2 : \begin{cases}\dot{X}_2 = f_2(x(t), u(t)) + \delta_2(t)\\ y_2 = C_2 X_2\end{cases} \tag{27}$$

where $X_1 = [x_1, x_2, x_3]^T$, $X_2 = [x_4, x_5, x_6]^T$, and

$$f_1(x(t), u(t)) = \begin{pmatrix}\dfrac{-R_1}{L_1}x_{11} + \dfrac{x_{21}}{L_1} - \dfrac{u_{\alpha_1}}{L_1}\\ \dfrac{-R_1}{L_1}x_{12} + \dfrac{x_{22}}{L_1} - \dfrac{u_{\beta_1}}{L_1}\\ \dfrac{x_{21}x_{11} + x_{22}x_{12}}{C_{eq}V_{dc_1}} - \dfrac{x_{13}}{C_{eq}}\\ -\dfrac{R_c}{L_c}x_{13} + \dfrac{V_{dc_1} - x_{23}}{L_c}\\ x_{32}\sqrt{x_{21}^2 + x_{22}^2}cos(x_{31})\\ x_{32}\sqrt{x_{21}^2 + x_{22}^2}sin(x_{31})\\ \dfrac{x_{13}}{C_{eq}} - \dfrac{x_{33}}{C_{eq}}\\ x_{31}\\ 0\\ 0\end{pmatrix};$$

$$\delta_1(t) = \begin{pmatrix} 0 \\ 0 \\ 0 \\ 0 \\ 0 \\ 0 \\ 0 \\ 0 \\ \delta_{11}(t) \\ \delta_{12}(t) \end{pmatrix} \tag{28}$$

and

$$f_2(x(t), u(t)) = \begin{pmatrix} \frac{-R_1}{L_1} x_{41} + \frac{x_{51}}{L_1} - \frac{u_{\alpha_2}}{L_1} \\ \frac{-R_1}{L_1} x_{42} + \frac{x_{52}}{L_1} - \frac{u_{\beta_2}}{L_1} \\ x_{62}\sqrt{x_{51}^2 + x_{52}^2}cos(x_{61}) \\ x_{62}\sqrt{x_{51}^2 + x_{52}^2}sin(x_{61}) \\ x_{61} \\ 0 \end{pmatrix};$$

$$\delta_2(t) = \begin{pmatrix} 0 \\ 0 \\ 0 \\ 0 \\ 0 \\ \delta_{21}(t) \end{pmatrix} \tag{29}$$

with the following notations:

$$\begin{aligned} u &= \begin{bmatrix} u_{\alpha_1} & u_{\beta_1} & u_{\alpha_2} & u_{\beta_2} \end{bmatrix}^T \\ x_1 &= \begin{bmatrix} x_{11} & x_{12} & x_{13} \end{bmatrix}^T = \begin{bmatrix} i_{\alpha_1} & i_{\beta_1} & i_c \end{bmatrix}^T \\ x_2 &= \begin{bmatrix} x_{21} & x_{22} & x_{23} \end{bmatrix}^T = \begin{bmatrix} e_{\alpha_1} & e_{\beta_1} & V_{dc_2} \end{bmatrix}^T \\ x_3 &= \begin{bmatrix} x_{31} & x_{32} & x_{33} \end{bmatrix}^T = \begin{bmatrix} \theta_1 & \omega_1 & i_{inv} \end{bmatrix}^T \\ x_4 &= \begin{bmatrix} x_{41} & x_{42} \end{bmatrix}^T = \begin{bmatrix} i_{\alpha_2} & i_{\beta_2} \end{bmatrix}^T \\ x_5 &= \begin{bmatrix} x_{51} & x_{52} \end{bmatrix}^T = \begin{bmatrix} e_{\alpha_2} & e_{\beta_2} \end{bmatrix}^T \\ x_6 &= \begin{bmatrix} x_{61} & x_{62} \end{bmatrix}^T = \begin{bmatrix} \theta_2 & \omega_2 \end{bmatrix}^T \end{aligned}$$

where u denotes is the input vector of the global system, x_1 and x_4 are the vector currents that are accessible for measurement. The vectors x_2 and x_5 are the electromagnetic variables of the two grids, and these variables are unavailable. The vectors x_3 and x_6, which group the grid parameters and the current absorbed by the inverter station, are unavailable. Generally, the variation of the network's pulsation is bounded, then its dynamic is supposed to be an unknown function $(\delta_{11}(t), \delta_{21}(t))$. Likewise, the dynamic of inverter current is assumed to be an unknown and bounded function $\delta_{11}(t)$. The relation between the electromagnetics variables in $(\alpha,\ \beta)$-coordinates and its magnitude E_1 and E_2 is given by:

$$\begin{aligned} E_1 &= \sqrt{e_{\alpha_1}^2 + e_{\beta_1}^2} = \sqrt{x_{21}^2 + x_{22}^2} \\ E_2 &= \sqrt{e_{\alpha_2}^2 + e_{\beta_2}^2} = \sqrt{x_{51}^2 + x_{52}^2} \end{aligned}$$

The electrical angle is estimated online using the well-known relationship:

$$\theta_i = \arctan\left(\frac{e_{\beta_i}}{e_{\alpha_i}}\right) \ ; \quad (i = 1, 2)$$

B. OBSERVER DESIGN FOR SUBSYSTEM $\mathbb{S}_1$

Subsystem (26) consists of an AC/DC converter and HVDC cable. The point is that not all state variables in subsystem $\mathbb{S}_1$ are accessible for measurement. On the grid side, the grid voltage and pulsation, and the electrical angle are not accessible to measurement. On the DC side, the HVDC cable output voltage V_{dc2} and the inverter current i_{inv} are not accessible for measurement. In order to obtain online estimates of these state variables, we will now design a state observer. Only the electrical grid currents and the input current of the HVDC cable are assumed to be available for measurement. And we assume that the output voltage of the rectifier station V_{dc1} is an external measured signal.

1) STATE TRANSFORMATION

We seek a state transformation $x \longrightarrow z$ that converts the $\mathbb{S}_1$ model (26) to a canonical triangular structure. One time the observer is developed in the z-coordinates (i.e, [31]), it will be re-expressed in the original x-coordinates for practical use, which has two advantages: (i) it simplifies observability analysis; (ii) it allows for the direct creation of high-gain observers.

Proposition 3: The transformation we are looking for is a diffeomorphis:

$$\varphi(x) : \mathbb{R}^9 \longrightarrow \mathbb{R}^9;\ x \longrightarrow z = \begin{pmatrix} z_{11} \\ z_{12} \\ z_{13} \end{pmatrix};\ \varphi(x) = \begin{pmatrix} \varphi_1(x) \\ \varphi_2(x) \\ \varphi_3(x) \end{pmatrix} \tag{30}$$

where $z_{11} = [x_{11}\ x_{12}\ x_{13}]^T$ is the measured vector. In view of (28) the dynamic of z_{11} is written as follows:

$$\dot{z}_{11} = z_{12} + \Phi_{11}(z_1, u) \tag{31}$$

with

$$\begin{aligned} z_{12} &= \begin{bmatrix} \frac{x_{21}}{L_1} & \frac{x_{22}}{L_1} & \frac{-x_{23}}{L_c} \end{bmatrix}^T \\ \Phi_{11}(z_1, u) &= \begin{pmatrix} \frac{-R_1}{L_1} & 0 & 0 \\ 0 & \frac{-R_1}{L_1} & 0 \\ 0 & 0 & \frac{-R_c}{L_c} \end{pmatrix} z_1 \\ &\quad + \begin{pmatrix} \frac{-1}{L_1} & 0 & 0 \\ 0 & \frac{-1}{L_1} & 0 \\ 0 & 0 & \frac{1}{L_c} \end{pmatrix} \begin{pmatrix} u_{\alpha_1} \\ u_{\beta_1} \\ V_{dc1} \end{pmatrix} \end{aligned} \tag{32}$$

In view of (32) and (28), the dynamics of the vector z_{12} are described by the equation:

$$\dot{z}_{12} = z_{13} + \Phi_{12}(z_{11}, z_{12}) \tag{33}$$

with

$$z_{13} = \begin{pmatrix} \frac{1}{L_1} x_{32} \sqrt{x_{21}^2 + x_{22}^2} cos(x_{31}) \\ \frac{1}{L_1} x_{32} \sqrt{x_{21}^2 + x_{22}^2} sin(x_{31}) \\ -\frac{x_{33}}{L_c C_2} \end{pmatrix}; \tag{34}$$

$$\Phi_{12}(z_1, z_2) = \begin{pmatrix} 0 & 0 & 0 \\ 0 & 0 & 0 \\ 0 & 0 & \frac{1}{L_c C_2} \end{pmatrix} z_{12} \tag{35}$$

It is easy to check that the dynamics of z_{13} can be written as:

$$\dot{z}_{13} = \Phi_{13}(x, u) + \beta(z)\delta_1(t) \tag{36}$$

with

$$\begin{aligned} \Phi_3(x, u) &= \frac{d\varphi_3(x)}{dx_{31}} \dot{x}_{31} \\ \beta(z)\delta_1(t) &= \frac{d\varphi_3(x)}{dx_{32}} \delta_{11}(t) + \frac{d\varphi_3(x)}{dx_{33}} \delta_{12}(t) \end{aligned} \tag{37}$$

in view of equations (31), (33), and (36) subsystem $\mathbb{S}_1$ is represented, in the z-coordinates, by the following compact form:

$$\begin{aligned} \dot{z}_1(t) &= Az_1(t) + \Phi(z_1, u) + D\beta(z)\delta_1(t) \\ y(t) &= C_1 z_1(t) = z_{11} \end{aligned} \tag{38}$$

where

$$A = \begin{bmatrix} \mathbb{O}_3 & \mathbb{I}_3 & \mathbb{O}_3 \\ \mathbb{O}_3 & \mathbb{O}_3 & \mathbb{I}_3 \\ \mathbb{O}_3 & \mathbb{O}_3 & \mathbb{O}_3 \end{bmatrix}; \; D = \begin{bmatrix} \mathbb{O}_3 \\ \mathbb{O}_3 \\ \mathbb{I}_3 \end{bmatrix}; \; C = \begin{bmatrix} \mathbb{I}_3 & \mathbb{O}_3 & \mathbb{O}_3 \end{bmatrix}$$

$$\Phi(z, u) = \begin{bmatrix} \Phi_1(z, u) \\ \Phi_2(z_1, z_2) \\ \Phi_3(x, u) \end{bmatrix}; \; \beta(z)\delta(t) = \begin{bmatrix} \frac{E_1}{L_1} cos(x_{31})\delta_{11} \\ \frac{E_1}{L_1} sin(x_{31})\delta_{11} \\ \frac{-1}{L_c C_2}\delta_{12} \end{bmatrix} \tag{39}$$

where $\mathbb{O}_n$ and $\mathbb{I}_n$ denoted the $(n \times n)$ null matrix and identity matrix, respectively. The high gain observer design method requires the following standard assumptions:

A 1: The function $\varphi(z, u)$ is globally Lipschitz in z uniformly in u.

A 2: The unknown function $\delta(t)$ is essentially bounded, i.e. there exists a scalar $\delta_0 > 0$, such that $\| \delta(t) \| \leq \delta_0$

Remark 3: Assumption 1 holds in practice because the state trajectory of all signals of the control system remains bounded.

2) OBSERVER DESIGN IN THE $Z-$COORDINATES

Consider the subsystem described by (26). As in [32], we propose for that subsystem the following high-gain observer:

$$\dot{\hat{z}}_1(t) = A_1 \hat{z}_1(t) + \phi(\hat{z}_1, u) - \lambda_1 \Delta_{\lambda_1}^{-1} K_1 C_1 (\hat{z}_1(t) - z_1(t)) \tag{40}$$

where $K_1 \in \mathbb{R}^{9\times 3}$ is the observer gain that is to be chosen such that the eigenvalues of matrix $(A_1 - K_1 C_1)$ is Hurwitz and Δ_{λ_1} is a diagonal matrix defined as follows:

$$\Delta_{\lambda_1} = diag\left(\mathbb{I}_3, \frac{1}{\lambda_1}\mathbb{I}_3, \frac{1}{\lambda_1^2}\mathbb{I}_3 \right) \tag{41}$$

with $\lambda_1 > 0$ is a real number.

Theorem 4: Under Assumptions **A.**1 and **A.**2, the high-gain observer given by (40), when applied to the z-system (30), is exponentially convergent for sufficiently large values of the gain λ_1. Specifically, there exists $\lambda_0 > 1$ such that for all $\lambda_1 > \lambda_0$ the observation error $\tilde{z}_1(t) = \hat{z}_1(t) - z_1(t)$ is asymptotically convergent to the origin.

Proof: Let us consider the observation error $\tilde{z}_1 = \hat{z}_1 - z_1$. From (38) and (40), it follows that this error is governed by the following equation:

$$\dot{\tilde{z}}_1 = (A_1 - \lambda_1 \Delta^{-1} K_1 C_1)\tilde{z}_1 + \phi(\hat{z}, u) - \phi(z, u) - D\delta(t) \tag{42}$$

Multiply both sides of (42) by Δ_{λ_1}, using the identities: $\Delta_{\lambda_1} A \Delta_{\lambda_1}^{-1} = \lambda_1 A$ and $C\Delta_{\lambda_1}^{-1} = C$, and introducing the variable change $\varepsilon_1 = \Delta_{\lambda_1}\tilde{z}_1$, we get from (42):

$$\dot{\varepsilon_1} = \lambda_1 (A_1 - K_1 C_1)\varepsilon_1 + \Delta_{\lambda_1}(\phi(\hat{z}, u) - \phi(z, u)) - \Delta_{\lambda_1} D\delta(t) \tag{43}$$

Now, let us choose the quadratic Lyapunov function $V(\varepsilon_1) = \varepsilon_1^T P \varepsilon_1$ with P any symmetric positive definite matrix. Differentiating V with respect to time gives, using (43):

$$\begin{aligned} \dot{V}(\varepsilon_1) &= 2\varepsilon_1^T P \dot{\varepsilon_1} \\ &= \lambda_1 \varepsilon_1^T P (A_1 - K_1 C_1)\varepsilon_1 + 2\varepsilon_1^T P \Delta_{\lambda_1}(\phi(\hat{z}, u) \\ &\quad - \phi(z, u) - D\delta(t)) \end{aligned} \tag{44}$$

Since the matrix $(A_1 - K_1 C_1)$, the matrix P can be chosen such that $(A_1 - K_1 C_1)^T P - P(A_1 - K_1 C_1) = -\mathbb{I}_9$. It is readily checked that:

$$\varepsilon_1^T \left((A - KC)^T P - P(A_1 - K_1 C_1) \right) \varepsilon_1 = - \| \varepsilon_1 \|^2 \tag{45}$$

where μ_{max} and μ_{min} are the largest and the smallest eigenvalues of the positive definite matrix P, respectively. Furthermore, using Assumptions 1 and 2, one has:

$$\begin{aligned} \| 2\Delta_{\lambda_1}(\phi(\hat{z}, u) - \phi(z, u)) \| &\leq \xi_1 \| \varepsilon_1 \| \\ \| \Delta_{\lambda_1} D\delta(t) \| &\leq \xi_2 \delta_0 \end{aligned} \tag{46}$$

where ξ_1 and ξ_2 are positive constants, and δ_0 is the upper limit of $\delta(t)$.

Also, as P is a positive definite matrix, the following inequality holds:

$$\mu_{min} \parallel \varepsilon_1 \parallel^2 \leq \varepsilon_1^T P \varepsilon_1 \leq \mu_{max} \parallel \varepsilon_1 \parallel^2 \tag{47}$$

Using (45), (46), and (47), it follows from (44) that:

$$\begin{aligned}\dot{V}(\varepsilon_1) &\leq -\frac{(\lambda_1 - \mu_{max}\xi_1)}{\mu_{min}} V(\varepsilon_1) + \frac{\mu_{max}\xi_2\delta_0}{\sqrt{\mu_{min}}}\sqrt{V(\varepsilon_1)} \\ &\leq -\gamma_1 V(\varepsilon_1) + \gamma_2\sqrt{V(\varepsilon_1)}\end{aligned} \tag{48}$$

For $\lambda_1 > \xi_1\mu_{max}$, where $\gamma_1 = \dfrac{\lambda_1 - \lambda_0}{\mu_{min}} > 0$; $\gamma_2 = \dfrac{\mu_{max}\xi_2\delta_0}{\mu_{min}}$. Introduce the variable change $W(\varepsilon_1) = \sqrt{V(\varepsilon_1)}$. It follows from (48) that W satisfy the following inequality:

$$\dot{W}(\varepsilon_1) \leq -\frac{\gamma_1}{2} W(\varepsilon_1) + \frac{\gamma_2}{2} \tag{49}$$

This demonstrates that $\dot{W}$ is negative whenever $W > \dfrac{\gamma_2}{\gamma_1}$. Therefore, for all $W(0)$ one has:

$$\limsup_{t \to +\infty} W(t) \leq \frac{\gamma_2}{\gamma_1} \tag{50}$$

which implies that $||\varepsilon||_P^2 < \left(\dfrac{\gamma_2}{\gamma_1}\right)^2$ is a region of attraction. Then, the proposed observer is globally asymptotically stable for whatever the initial conditions $z_1(0)$. It turns out that the observation error $\tilde{z}_1(t) = \hat{z}_1(t) - z_1(t)$ converges exponentially to a compact neighborhood of the origin and the size of that neighborhood can be made arbitrarily small by letting the observer gain λ_1 be sufficiently large.

This completes the proof of Thoerem 4.

3) OBSERVER DESIGN IN THE X-COORDINATES

For implementation purposes, the observer developed in the previous subsection must be represented in the original x-coordinates. The resulting x-coordinates observer is stated in the following theorem:

Theorem 5: The state observer (40) expresses in the x-coordinates:

$$\dot{\hat{X}}_1(t) = f(\hat{X}_1(t), u) - \lambda_1 \Delta_{\lambda_1}^{-1} J_1^{-1} K_1 C_1 (\hat{X}_1(t) - X_1(t)) \tag{51}$$

where Δ_1 and C_1 are respectively given by (41) and (39), and J_1 is the Jacobian of the transformation (30).

Proof: Recall the definition of the Jacobian is denoted as follows:

$$J_1 = \frac{d\varphi_1(x)}{dx} = \begin{bmatrix} \dfrac{\partial\varphi_{11}(x)}{\partial x_1} & \dfrac{\partial\varphi_{11}(x)}{\partial x_2} & \dfrac{\partial\varphi_{11}(x)}{\partial x_3} \\ \dfrac{\partial\varphi_{12}(x)}{\partial x_1} & \dfrac{\partial\varphi_{12}(x)}{\partial x_2} & \dfrac{\partial\varphi_{12}(x)}{\partial x_3} \\ \dfrac{\partial\varphi_{13}(x)}{\partial x_1} & \dfrac{\partial\varphi_{13}(x)}{\partial x_2} & \dfrac{\partial\varphi_{13}(x)}{\partial x_3} \end{bmatrix} \tag{52}$$

To determine the observability condition, we will analyze the Jacobian matrix. One can easily check that the $det(J_1) = \dfrac{1}{L_1^4 L_c C_2}(E_1\omega_1)^2$, it's clear that this determinant vanishes only if the grid voltage does so (no electric power in the grid).

Using the transformation (30) $z_1 = \varphi_1(x)$, the time-derivative of $\hat{z}_1$ undergoes the following equation:

$$\dot{\hat{z}}_1 = \frac{d\varphi_1(\hat{x})}{d\hat{x}}\frac{d\hat{x}}{dt} = J_1\frac{d\hat{x}}{dt} \implies \dot{\hat{x}} = J_1^{-1}\dot{\hat{z}} \tag{53}$$

In view to (26), (30) and (38), it follows immediately that: $f(\hat{x}, u) = J_1^{-1}(A\hat{z} + \varphi_2(\hat{z}, u))$. Using (53) and (40), the system (51) is a high gain observer for the subsystem represented by (26). This ends the proof of Thoerem (5).

C. OBSERVER DESIGN FOR SUBSYSTEM $\mathbb{S}_2$

Subsystem (27) consists of an inverter station connected to the AC network. In this subsystem, only some of the state variables are available. Electrical currents are considered to be the only ones that can be measurably available. Conversely, the grid voltage, pulsation, and electrical position are not accessible for measurement. Consequently, the objective is to design an observer who provides online estimates of the state variables e_{α_2}, e_{β_2}, θ_2, and ω_2. To this end, a state observer is synthesized following the same steps as the above observer for subsystem (26).

1) OBSERVER DESIGN

The following system is a high gain observer for the susbsystem (27):

$$\dot{\hat{X}}_2(t) = f_2(\hat{X}(t), u) - \lambda_2 \Delta_{\lambda_2} J_2^{-1} K_2 C_2 (\hat{X}_2(t) - X_2(t)) \tag{54}$$

Theorem 6: Consider the subsystem represented by the nonlinear model (27), where δ_2 is considered a bounded signal. There are real positives constants (q_1, q_2, q_3), and large λ_2, such that $\forall\lambda_2 > \lambda_0$ the estimation error $\tilde{X}_2$ is globally convergent and satisfies the following inequality:

$$\|\hat{X}_2(t) - X_2(t)\| \leq q_1 \|\hat{X}_2(t_0) - X_2(t_0)\| e^{-q_2(t-t_0)} + q_3$$

Consequently, the observation error $\tilde{X}_2$ can be made arbitrarily small letting λ_2 be sufficiently large, whatever the initial conditions.

Proof: Therefore, according to Theorem (4), The system (54) is a high-gain observer for the subsystem (27). This ends with the proof of Theorem (6).

D. OUTPUT FEEDBACK CONTROLLER

The whole output feedback controller is obtained by combining the state feedback (16), (19), (23), (24) and the observer (51), (54). Doing so, one gets the following output feedback control law:

$$u_{d_1} = \frac{L_1}{\beta}\left[e_3 + c_4 e_4 + \beta(-\frac{R_1}{L_1}\bar{x}_6 + \hat{\omega}_1\bar{x}_7 + \frac{\hat{e}_{d_1}}{L_1}) - \dot{\alpha}_3\right] \tag{55}$$

TABLE 1. The summary table presenting the suggested output feedback controller.

Studied system	$\dot{x} = f(x,u)$ (59) with $f(x,u)$ represents the compacted version (4.1)-(4.7)
Observer	$\dot{\hat{X}}_1(t) = f_1(\hat{X}_1(t),u) - \lambda_1 \Delta_{\lambda_1}^{-1} J_1^{-1} K_1 C_1 (\hat{X}_1(t) - X_1(t))$ (60) $\dot{\hat{X}}_2(t) = f_2(\hat{X}_2(t),u) - \lambda_2 \Delta_{\lambda_2}^{-1} J_2^{-1} K_2 C_2 (\hat{X}_2(t) - X_2(t))$ (61) with f_1 f_2 $J_{1,2}$ and $\Delta_{\lambda_{1,2}}$ are defined in (28), (28), (51), and (40) and $K_{1,2}$ is the gains of the proposed observers selected such that the matrices $(A_{1,2} - K_{1,2}C_{1,2})$ are hurwitz
Control laws	$u_{d_1} = \frac{L_1}{\beta}\left[e_3 + c_4 e_4 + \beta(-\frac{R_1}{L_1}\bar{x}_4 + \hat{\omega}_1 \bar{x}_5 + \frac{\hat{e}_{d_1}}{L_1}) - \dot{\alpha}_3\right]$ (62) $u_{q_1} = \frac{1}{L_1}\left[\frac{c_5 e_5}{\hat{e}_{d_1}} - \frac{R_1}{L_1}\bar{x}_5 - \hat{\omega}_1 \bar{x}_4\right]$ (63) $u_{d_2} = L_2\left[-c_6 e_6 + \frac{R_2}{L_2}\bar{x}_6 - \hat{\omega}_2 \bar{x}_7 + \frac{\hat{e}_{d_2}}{L_2} + \dot{x}_6^*\right]$ (64) $u_{q_2} = L_2\left[-\frac{c_7 e_7}{\hat{e}_{d_2}} + \frac{R_2}{L_2}\bar{x}_7 + \hat{\omega}_2 \bar{x}_6\right]$ (65)

$$u_{q_1} = \frac{1}{L_1}\left[\frac{c_5 e_5}{\hat{e}_{d_1}} - \frac{R_1}{L_1}\bar{x}_5 - \hat{\omega}_1 \bar{x}_4\right] \tag{56}$$

$$u_{d_2} = L_2\left[-c_6 e_6 + \frac{R_2}{L_2}\bar{x}_6 - \hat{\omega}_2 \bar{x}_7 + \frac{\hat{e}_{d_2}}{L_2} + \dot{x}_6^*\right] \tag{57}$$

$$u_{q_2} = L_2\left[-\frac{c_7 e_7}{\hat{e}_{d_2}} + \frac{R_2}{L_2}\bar{x}_7 + \hat{\omega}_2 \bar{x}_6\right] \tag{58}$$

For convenience, the whole output feedback controller equations are recapitulated in Table 1:

V. SIMULATION RESULTS

To validate the efficiency and superiority of the proposed control technique, the experimental setup shown in Fig. 3 is simulated using MATLAB/Simulink 2018a. The controlled part is two converter stations connected via an HVDC cable, and each converter has the same AC system interface with the numerical parameters given in Table 2, and the controller and observer parameters design are given in Table 3. Then, the controllers (16), (19),(23), (24), and the observers (51), (54) have been implemented under Digital Signal Processor (DSP) using the Embedded Coder Support Package for Texas Instruments c2000 for auto code generation of the process in the loop test (PIL). This semi-experimental setup is intended to highlight runtime problems in the embedded system. Additionally, the whole VSC-HVDC system model is performed on the host PC, while the generated code from the Simulink blocks runs directly on the target hardware. They communicate with one another using an RS-332 cable and Serial Communications Interface (SCI).

In fact, the control performances depend on the numerical values given to the controller and observer parameters, *i.e.*, $c_1, \ldots, c_7$, $\lambda_{1,2}$, and $K_{1,2}$. The point is that there is no systematic approach, particularly in nonlinear control, to select appropriate choices for these values. As a result, the standard procedure is to use a trial-and-error method. Then, the following numerical values are obtained as shown in Table 3.

Remark 7: The observers gain $K_{1,2}$ are chosen so that the state matrices $(A_{1,2} - K_{1,2}C_{1,2})$ are Hurwitz, and the values of $\lambda_{1,2}$ are chosen high sufficiently to assure that the observer converges more quickly than the controller.

TABLE 2. VSC-HVDC system characteristics.

Characteristics	Symbol	Values
AC networks		
Voltage	$E_1 = E_2$	$220\,KV$
Frequency	$f_1 = f_2$	$50\,Hz$
VSCs Station		
Resistor	$R_1 = R_2$	$0.48\,\Omega$
Inductor	$L_1 = L_2$	$45\,mH$
Capacitor	$C_1 = C_2$	$500\,\mu F$
HVDC cable		
Resistor	R_c	$7\,m\Omega$
Capacitor	C_c	$50\,\mu F$
Inductor	L_c	$0.11\,mH$

TABLE 3. Observer-controller design parameters.

Observers Parameters	$\lambda_1 = 1200, \lambda_2 = 900$ $K_1 = \begin{bmatrix} 3\mathbb{I}_{3\times3} & \mathbb{I}_{3\times3} & \mathbb{I}_{3\times3} \end{bmatrix}$ $K_2 = \begin{bmatrix} 3\mathbb{I}_{2\times2} & \mathbb{I}_{2\times2} & \mathbb{I}_{2\times2} \end{bmatrix}$
Controller Parameters	$c_1 = 100; c_2 = 200; c_3 = 600; c_4 = 500;$ $c_5 = 2000; c_6 = 700; c_7 = 500.$

A. ILLUSTRATION UNDER NORMAL CONDITIONS

The performances of the proposed output feedback controller are tested under normal network conditions: the grids frequency $f_1 = 50\,Hz$, $f_2 = 50\,Hz$ and the grids voltage $E_1 = 220\,KV$, $E_2 = 220\,KV$. Also, the active power undergoes a change of 30 % of its nominal value at $t = 1\,s$.

Figure 4 presents the tracking performances of the proposed output feedback control. Fig. 4a shows the behavior

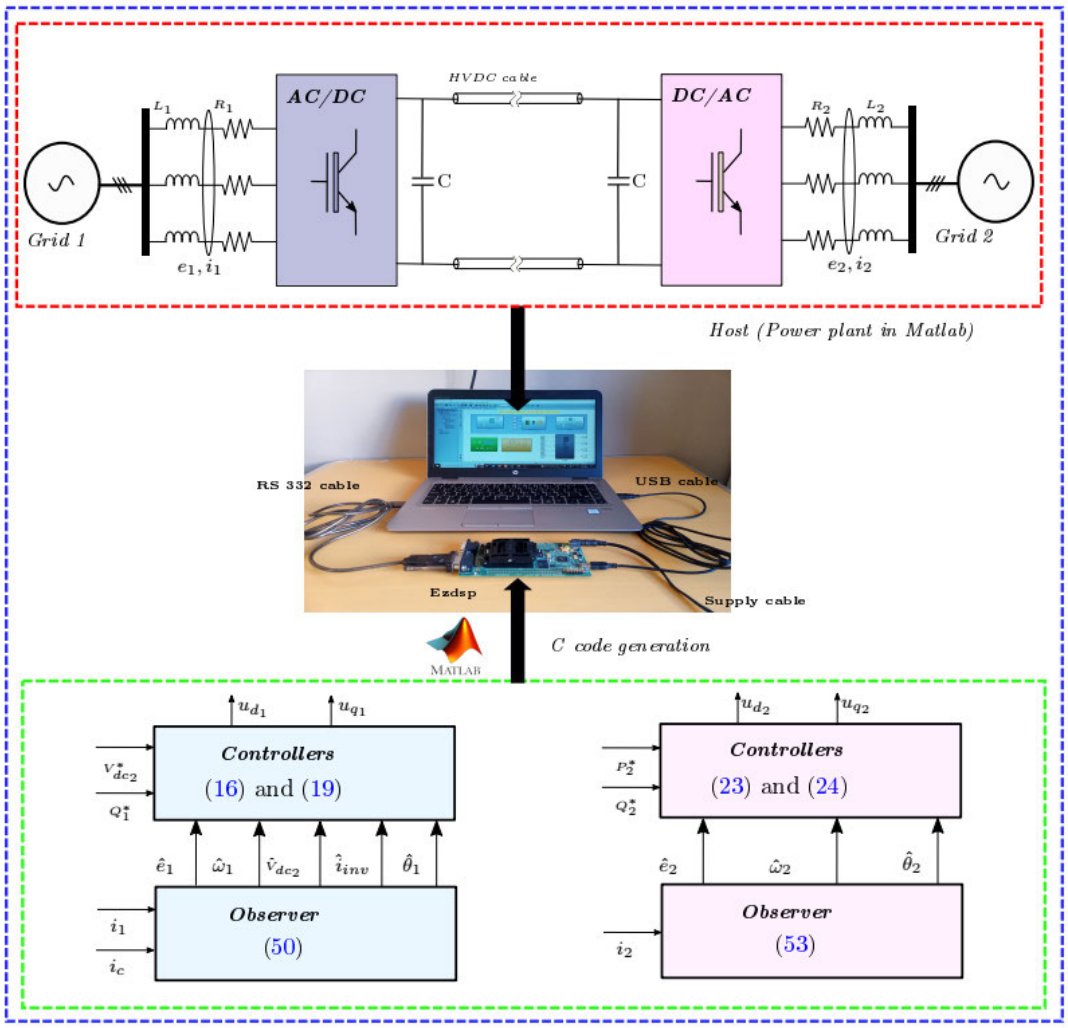

FIGURE 3. The system output feedback control scheme.

TABLE 4. Quality assessment measures for both control strategies.

Approach	$V^*_{dc_2} - V_{dc_2}$				$P^*_2 - P_2$			
	ISE	*ITSE*	*IAE*	*ITAE*	*ISE*	*ITSE*	*IAE*	*ITAE*
BSC	$4.146\,e^{-6}$	$4.201\,e^{-6}$	$1\,e^{-3}$	$1\,e^{-3}$	0.012	0.02	0.5	1.03
PI	$5\,e^{-3}$	$5\,e^{-3}$	$2.4\,e^{-3}$	$2.4\,e^{-3}$	1.3	2.41	1.21	4.13

of DC voltage V_{dc_1} and V_{dc_2}, it can see the voltage (V_{dc_2}) at the end of the HVDC cable is precisely follows the reference signal. While Fig. 4b presents the active power P_2. Despite the power change at time 1s, it is clear that the active power P_2 totally converges to its reference signal.

The voltage and current of line a of the grids on both sides are presented in Figs. 4c and 4e. The currents remain sinusoidal and in phase with the supply voltages, meeting PFC requirements. This indicates that the reactive power has been suspended, as shown in Figs. 4d and 4f.

The performances of the proposed observer(51) are illustrated in Figure 5. Figs. 5a and 5b show that the voltage e_{α_1} and e_{β_1} of grid 1 match well with their measured signals, and the estimation error disappears completely after a short time. Figures. 5c and 5d are present the grid electrical angle and the grid pulsation, it is clear that the estimated values converge quickly to their true values. Additionally, the HVDC cable output voltage and the inverter current are illustrated in Figures. 5e and 5f. It is seen that the estimated values, provided by the observer (51), match well their true values, and the estimation error vanished after a short time. The performances of the proposed observer(54) are illustrated in Figure 6. Figure. 6a and 6b show that the voltage e_{α_2} and e_{β_2} of grid 2 match well to their measured signals, and the estimation error vanished after a short time. Fig 6c and 6d are presented the grid electrical angle and the grid pulsation. It is clear that the estimated values converge quickly to their true values.

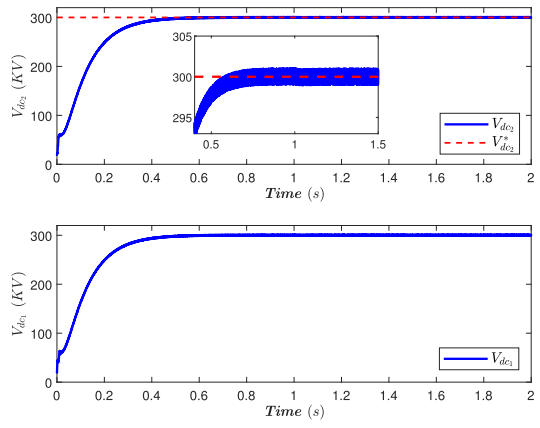

(a) DC voltages (V_{dc_2}, V_{dc_1})

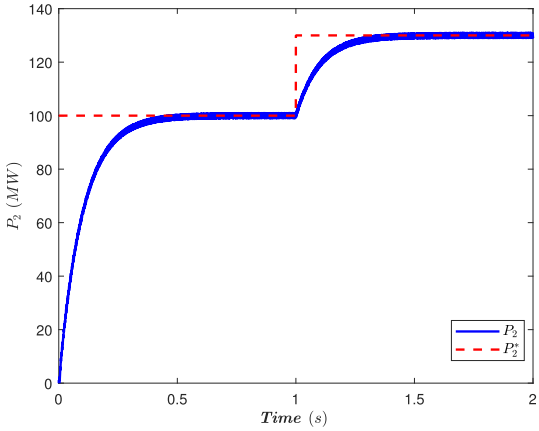

(b) Active power P_2

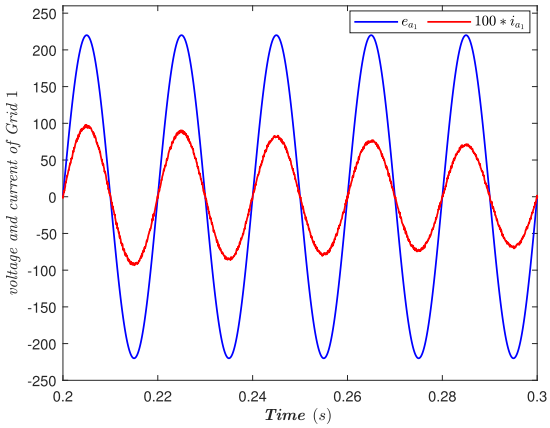

(c) Current and voltage of grid 1 line a

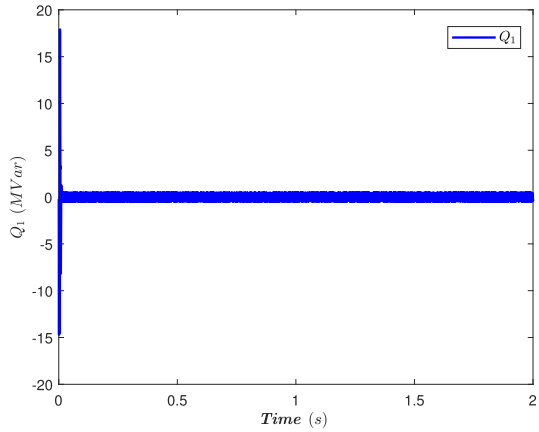

(d) Reactive power of grid 2 (Q_1)

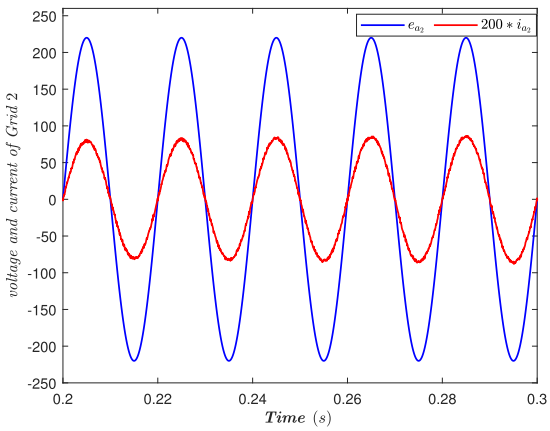

(e) Current and voltage of grid 2 line a

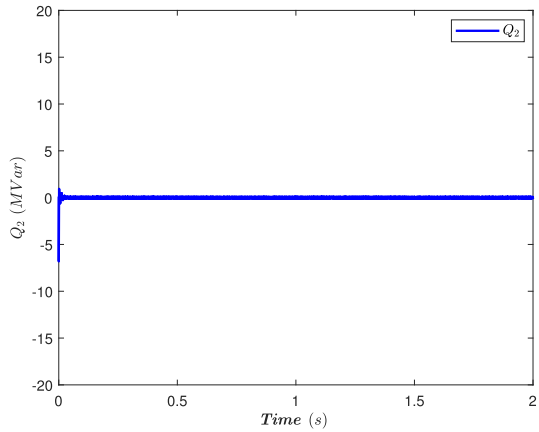

(f) Reactive power of grid 2 (Q_2)

FIGURE 4. The tracking performances of the output feedback control.

B. COMPARATIVE STUDY ANALYSIS

To assess the effectiveness of the suggested backstepping controller (BSC) in comparison to other innovative techniques, such as the PI controller. Figs. 7a and 7b represent the resultant performances of the two controllers. Clearly, the new controller outperforms the PI controller in terms of performance. Notably, it excels in reference tracking, leading to significantly shorter transients. The superiority of the new controller is underscored by the data presented in Table 4, where the performance is related to a different quality control criterion (tracking error specification).

C. POWER GRID FLUCTUATIONS

In fact, the amplitude and pulsation of the voltage of both power grids are subject to fluctuations. So that the proposed output feedback performance will be tested under a voltage

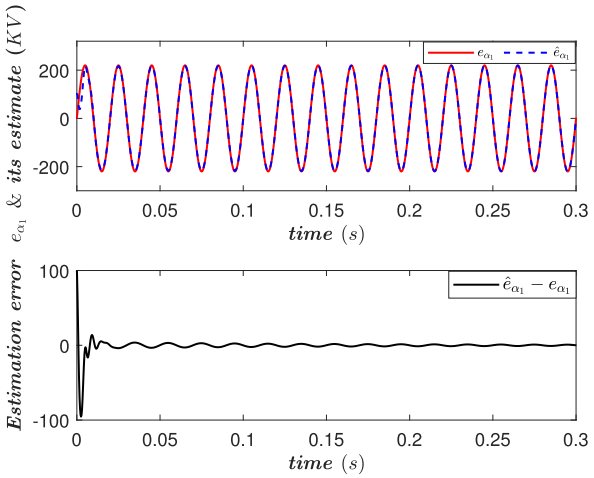

(a) **Top:** α_1-Axis voltage, the true e_{α_1} and its estimate $\hat{e}_{\alpha_1}$. **Bottom:** Estimation error

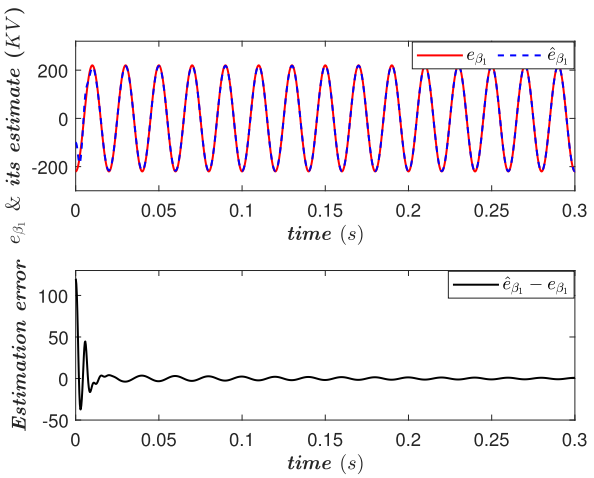

(b) **Top:** β_1-Axis voltage, the true e_{β_1} and its estimate $\hat{e}_{\beta_1}$. **Bottom:** Estimation error

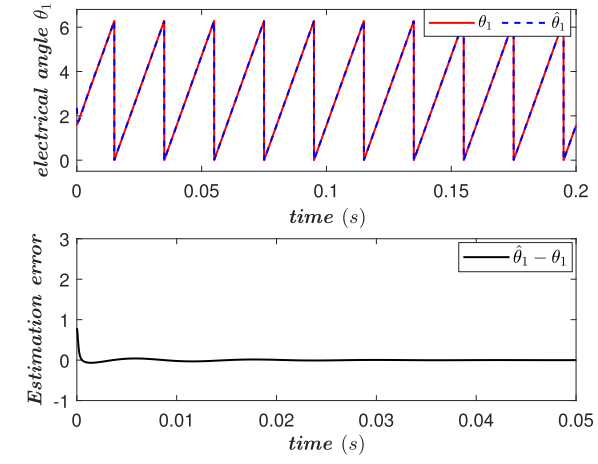

(c) **Top:** The electrical angle θ_1 and its estimate $\hat{\theta}_1$. **Bottom:** Estimation error

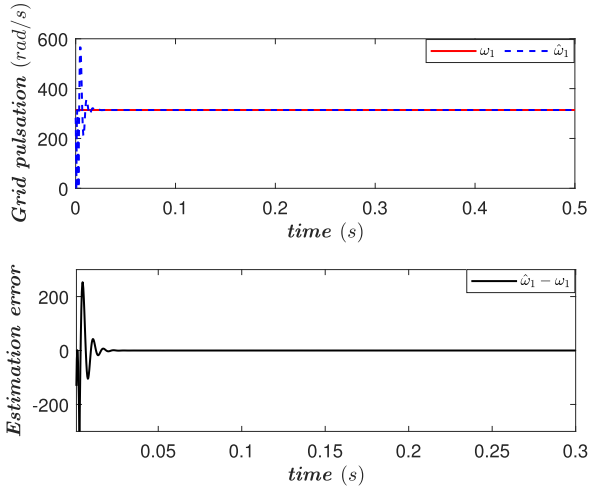

(d) **Top:** The grid pulsation ω_1 and its estimate $\hat{\omega}_1$. **Bottom:** Estimation error

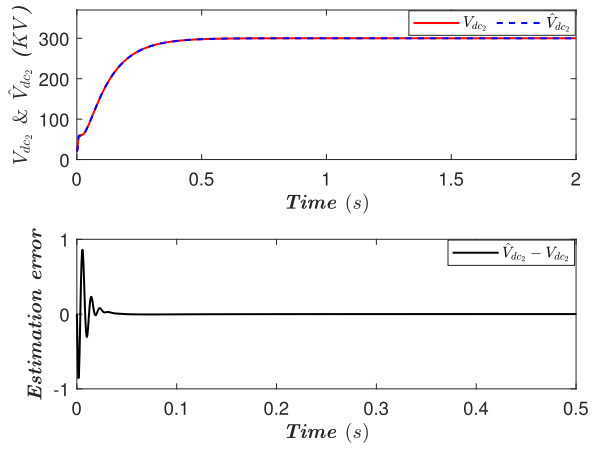

(e) **Top:** The true voltage V_{dc_2} and its estimate $\hat{V}_{dc_2}$. **Bottom:** Estimation error

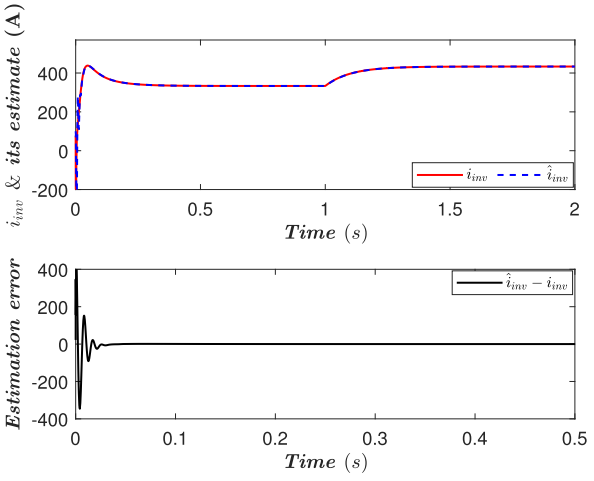

(f) **Top:** The inverter current i_{inv} and its estimate $\hat{i}_{inv}$. **Bottom:** Estimation error

FIGURE 5. **Tracking performance of the proposed Observer (51) for terminal 1 side under normal condition.**

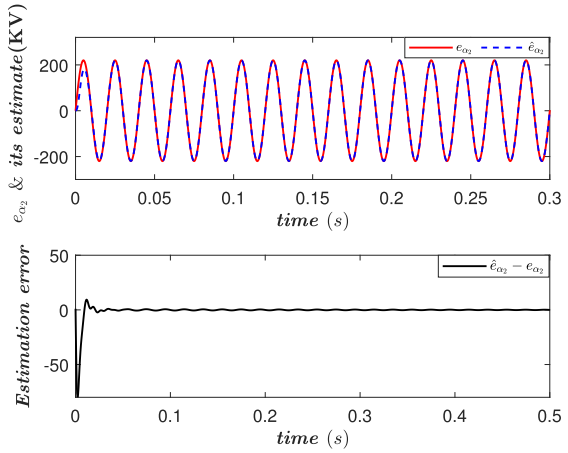

(a) **Top:** α_2-Axis voltage, the true e_{α_2} and its estimate $\hat{e}_{\alpha_2}$. **Bottom:** Estimation error

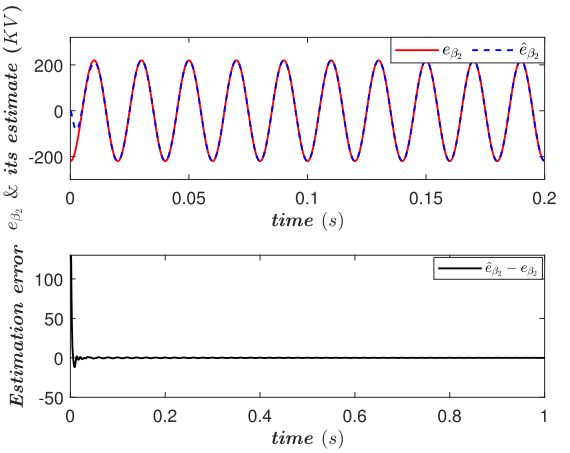

(b) **Top:** β_2-Axis voltage, the true e_{β_2} and its estimate $\hat{e}_{\beta_2}$. **Bottom:** Estimation error

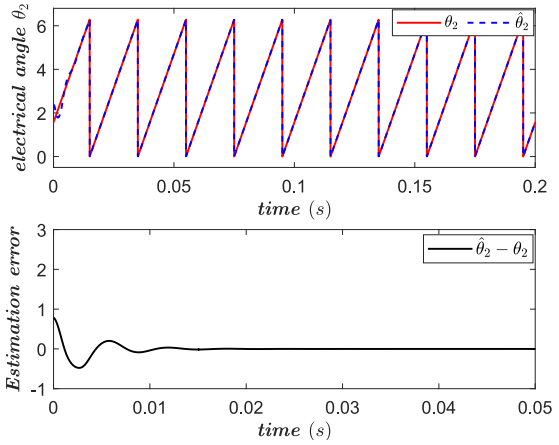

(c) **Top:** The electrical angle θ_2 and its estimate $\hat{\theta}_2$. **Bottom:** Estimation error

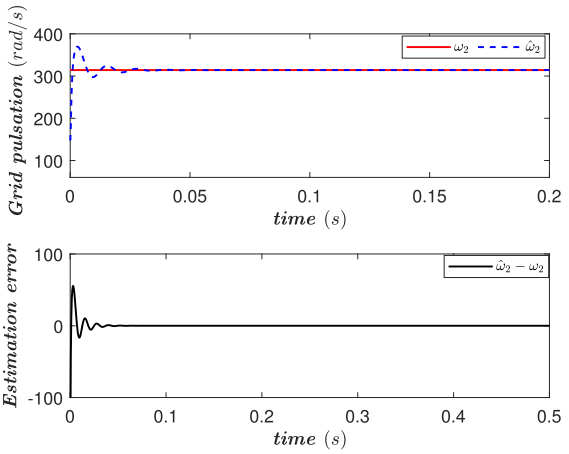

(d) **Top:** The grid pulsation ω_2 and its estimate $\hat{\omega}_2$. **Bottom:** Estimation error

FIGURE 6. **Tracking performance of the proposed Observer (54) for terminal 2 side under normal condition.**

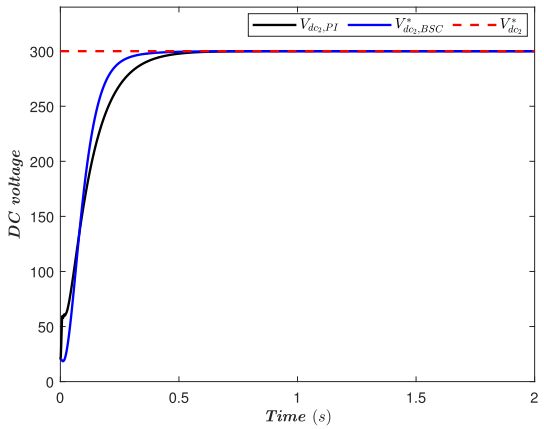

(a) Votage V_{dc_2}

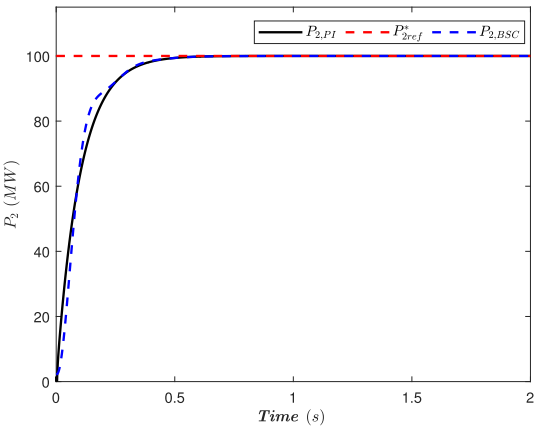

(b) Power P_2

FIGURE 7. **Tracking performances of BSC and PID controllers.**

and pulsation variation of both grids. When the pulsations (ω_1, ω_2) are subject to a variation of $+10\,\%$ at $[0.2\ \ 0.4]\,s$ and a variation of $-10\,\%$ at $[0.4\ 0.6]\,s$ of nominal pulsations (See Figs. 8b and 9b),), and when the voltages (E_1, E_2) are

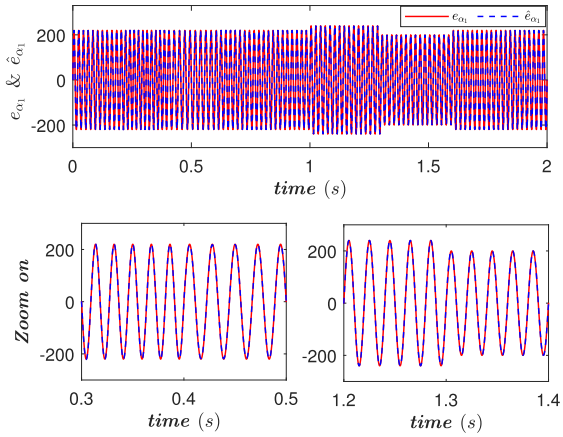

(a) **Top:** α_2-Axis voltage, the true e_{α_2} and its estimate $\hat{e}_{\alpha_2}$. **Bottom:** Estimation error

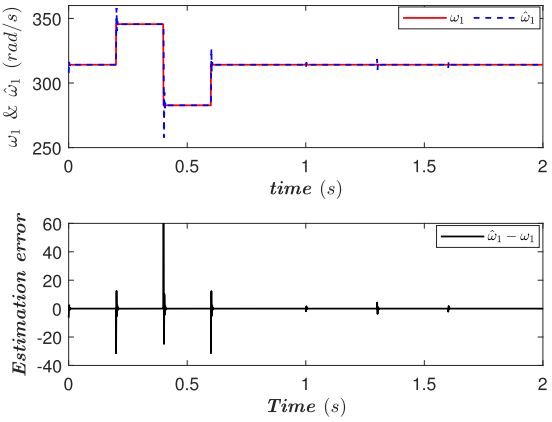

(b) **Top:** The grid pulsation ω_2 and its estimate $\hat{\omega}_2$. **Bottom:** Estimation error

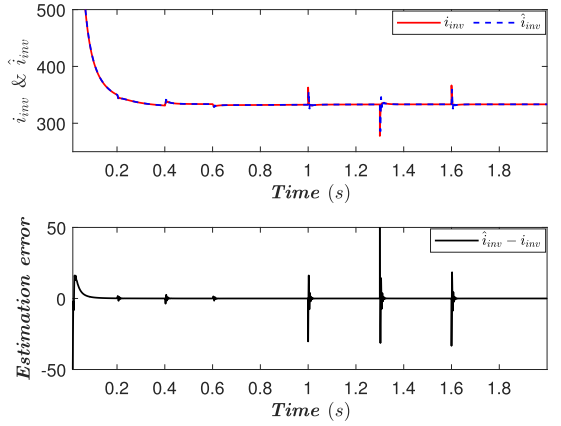

(c) **Top:** The inverter current i_{inv} and its estimate $\hat{i}_{inv}$. **Bottom:** Zoom on

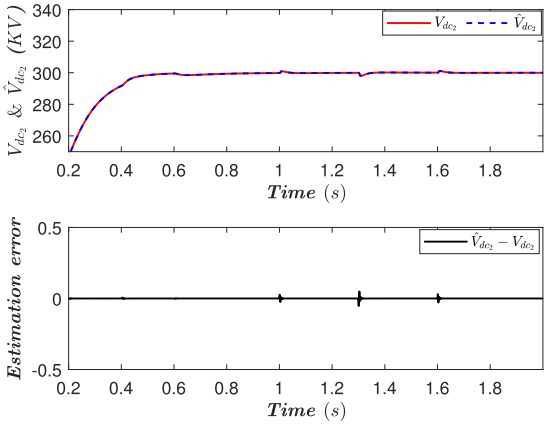

(d) **Top:** The true voltage V_{dc_2} and its estimate $\hat{V}_{dc_2}$. **Bottom:** Estimation error

FIGURE 8. **Tracking performance of the proposed observer (54) under grid fluctuations.**

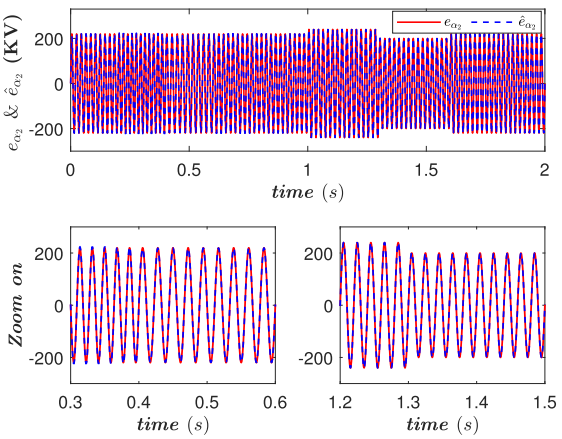

(a) **Top:** α_2-Axis voltage, the true e_{α_2} and its estimate $\hat{e}_{\alpha_2}$. **Bottom:** Zoom on

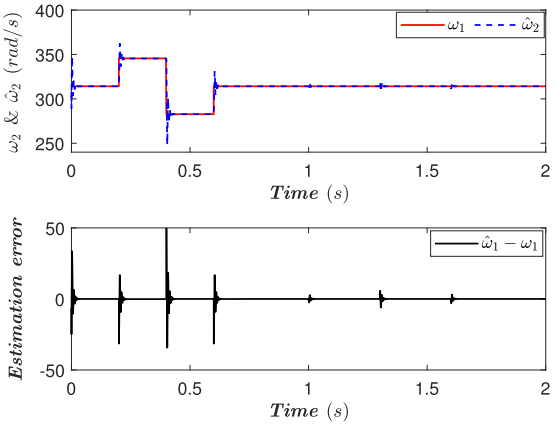

(b) **Top:** The grid pulsation ω_2 and its estimate $\hat{\omega}_2$. **Bottom:** Estimation error

FIGURE 9. **Tracking performance of the proposed observer (54) under grid fluctuations.**

increased of $+30\,\%$ at $[1\ \ 1.3]\,s$ and decreased by $-30\,\%$ at $[1.3\ \ 1.6]\,s$ of the nominal voltages (See Figs. 8a and Figs. 9a).

More specifically, Figs. 8 and 9 show that the online estimation provided by the observers rapidly converges to

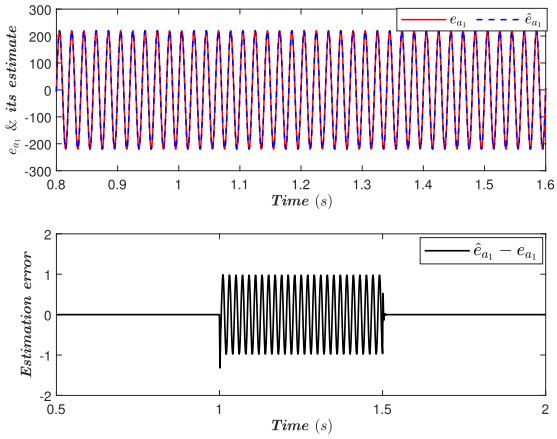

(a) Zoom on the grid voltage e_{a_1} and its estimation error

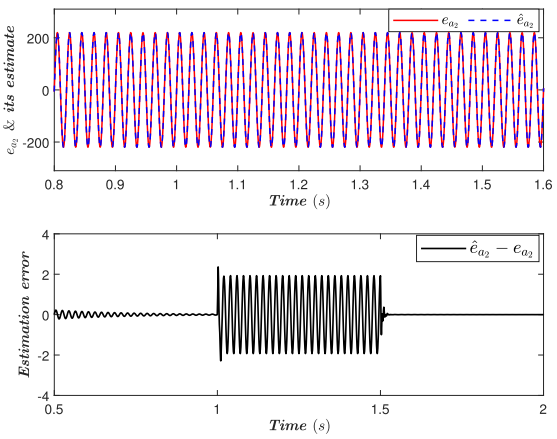

(b) Zoom on the grid voltage e_{a_2} and its estimation error

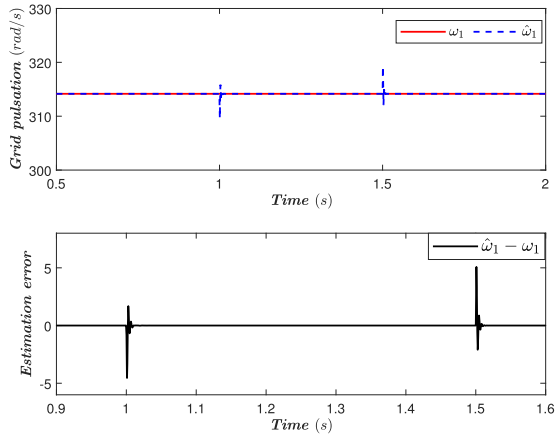

(c) The grid pulsation ω_1 and its estimation error

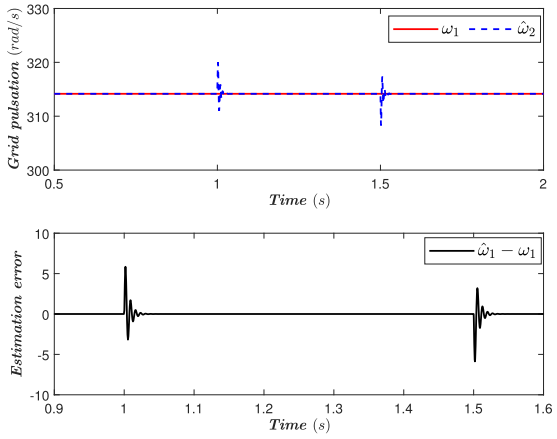

(d) The grid pulsation ω_2 and its estimation error

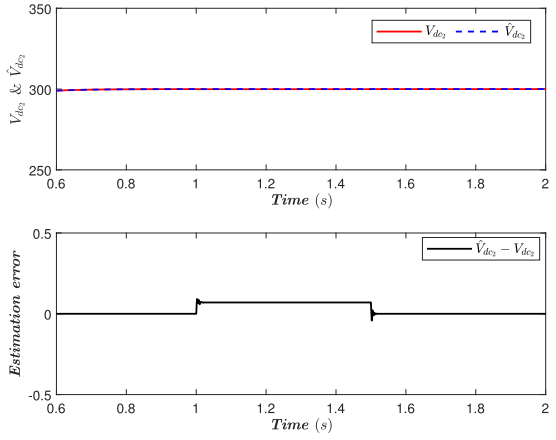

(e) The voltages $(V_{dc_2}\ \hat{V}_{dc_2})$ and its estimation error

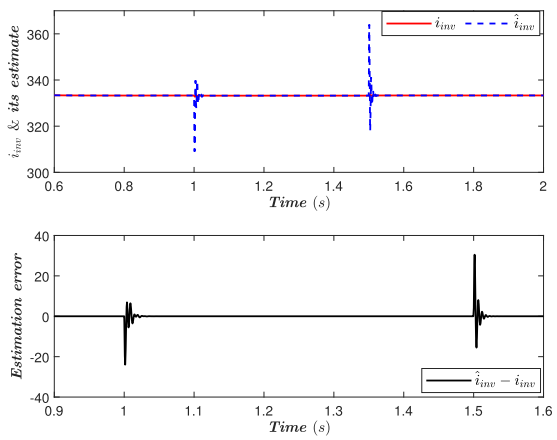

(f) The inverter current i_{inv} and its estimation error

FIGURE 10. **Robustness test of the observers: grids impedance and HVDC cable impedance uncertainties.**

their true values despite the variation in the grids voltage and pulsation.

D. VARIATION OF CHARACTERISTICS ON THE AC AND DC SIDES

To verify the robustness of the proposed output feedback controller against system characteristics variation,

In our study, we analyze the dynamic behavior of the system while considering a 30% uncertainty in the nominal values of both the grid impedances and the HVDC cable impedance. During the time interval from [1 1.5] seconds, we apply the true values of these parameters in our simulated HVDC model. In contrast, we utilize the nominal values when implementing the proposed state observer. The performances

of observers are shown in Figs. 10a - 10f After a brief transitory period, all the estimated states reach their true values, indicating that the observers are still performing properly.

VI. CONCLUSION

In summary, this work has introduced a nonlinear output feedback control method for a two-terminal VSC HVDC transmission system. The designed system involves two electrical grids, each connected to a VSC-based converter station. These converter stations are interlinked via a lengthy HVDC cable. Firstly, a multi-loops nonlinear controller has been designed based on the backstepping approach and Lyapunov stability tools. Then, two nonlinear observers are proposed to provide online estimates of all electrical state variables in the HVDC system. Such as the grids voltage and frequency as well as the electrical angle on the AC side, and the states of the HVDC cable as well the inverter current are provided by the proposed observers. The line currents are considered to be the only ones needed for measuring. Based on these estimations, the output feedback controller can be developed. Finally, numerous simulations have verified that the provided output feedback control ensures the accomplishment of control objectives with exceptional performance, including: (i) precise regulation of continuous voltage in the HVDC cable, (ii) nearly optimal power factor for both grids, and (iii) effective regulation of active power for the second grid. Using a rigorous test methodology that includes common grid issues (voltage and frequency variation) and the change of the system characteristics, The obtained results show that the proposed output feedback control achieves all control objectives with excellent performances.

REFERENCES

[1] A. S. Ayobe and S. Gupta, "Comparative investigation on HVDC and HVAC for bulk power delivery," *Mater. Today, Proc.*, vol. 48, pp. 958–964, Jan. 2022.

[2] S. Khalid, A. Raza, M. Z. Yousaf, S. Mirsaeidi, and C. Zhichu, "Recent advances and future perspectives of HVDC development in Pakistan: A scientometric analysis based comprehensive review," *IEEE Access*, vol. 11, pp. 56408–56427, 2023.

[3] W. Wang, G. Li, and J. Guo, "Large-scale renewable energy transmission by HVDC: Challenges and proposals," *Engineering*, vol. 19, pp. 252–267, Dec. 2022.

[4] I. El Myasse, A. Mansouri, A. El Magri, A. Watil, M. Kissaoui, R. Lajouad, S. Ashfaq, and N. Elaadouli, "Robust nonlinear control design of MMC-HVDC systems for wind power plants integration," in *Proc. 3rd Int. Conf. Innov. Res. Appl. Sci., Eng. Technol. (IRASET)*, May 2023, pp. 1–5.

[5] H. Xiao, K. Sun, J. Pan, Y. Li, and Y. Liu, "Review of hybrid HVDC systems combining line communicated converter and voltage source converter," *Int. J. Electr. Power Energy Syst.*, vol. 129, Jul. 2021, Art. no. 106713.

[6] J. K. Pradhan, A. Ghosh, and C. N. Bhende, "Small-signal modeling and multivariable PI control design of VSC-HVDC transmission link," *Electr. Power Syst. Res.*, vol. 144, pp. 115–126, Mar. 2017.

[7] D. Zonetti, R. Ortega, and A. Benchaib, "Modeling and control of HVDC transmission systems from theory to practice and back," *Control Eng. Pract.*, vol. 45, pp. 133–146, Dec. 2015.

[8] I. El Myasse, A. El Magri, M. Kissaoui, R. Lajouad, F. Giri, A. Watil, and L. Bahatti, "Observer and nonlinear control design of VSC-HVDC transmission system," *Int. J. Electr. Power Energy Syst.*, vol. 145, Feb. 2023, Art. no. 108609. [Online]. Available: https://www.sciencedirect.com/science/article/pii/S0142061522006056

[9] J. Stojković, A. Lekić, and P. Stefanov, "Adaptive control of HVDC links for frequency stability enhancement in low-inertia systems," *Energies*, vol. 13, no. 23, p. 6162, Nov. 2020.

[10] I. González-Torres, H. Miranda-Vidales, J. Espinoza, C.-F. Méndez-Barrios, and M. González, "State feedback control assisted by a gain scheduling scheme for three-level NPC VSC-HVDC transmission systems," *Electric Power Syst. Res.*, vol. 157, pp. 227–237, Apr. 2018.

[11] E. Kamal, "Stabilization of large power systems using VSC-HVDC and fuzzy anti-windup subject to input constraints," *Electr. Power Compon. Syst.*, vol. 48, nos. 6–7, pp. 572–588, Apr. 2020, doi: 10.1080/15325008.2020.1797933.

[12] D.-H. Kwon and Y.-J. Kim, "Optimal data-driven control of an LCC HVDC system for real-time grid frequency regulation," *IEEE Access*, vol. 8, pp. 58470–58482, 2020.

[13] M. S. Alam, M. A. Abido, and Z. M. Al-Hamouz, "Model predictive control approach for bridge-type fault current limiter in VSC-HVDC system," *Arabian J. Sci. Eng.*, vol. 44, no. 3, pp. 2079–2089, Mar. 2019.

[14] A. Shetgaonkar, L. Liu, A. Lekić, M. Popov, and P. Palensky, "Model predictive control and protection of MMC-based MTDC power systems," *Int. J. Electr. Power Energy Syst.*, vol. 146, Mar. 2023, Art. no. 108710.

[15] X. Zheng, Y. Li, Z. Liu, and C. Wang, "Steady-state control strategy of VSC-HVDC transmission system based on full-order terminal sliding mode control method," *J. Eng.*, vol. 2019, no. 16, pp. 987–990, Mar. 2019.

[16] D. Zonetti, G. Bergna-Diaz, R. Ortega, and N. Monshizadeh, "PID passivity-based droop control of power converters: Large-signal stability, robustness and performance," *Int. J. Robust Nonlinear Control*, vol. 32, no. 3, pp. 1769–1795, Feb. 2022.

[17] B. Yang, L. Jiang, T. Yu, H. C. Shu, C.-K. Zhang, W. Yao, and Q. H. Wu, "Passive control design for multi-terminal VSC-HVDC systems via energy shaping," *Int. J. Electr. Power Energy Syst.*, vol. 98, pp. 496–508, Jun. 2018.

[18] D. Dong, B. Wen, D. Boroyevich, P. Mattavelli, and Y. Xue, "Analysis of phase-locked loop low-frequency stability in three-phase grid-connected power converters considering impedance interactions," *IEEE Trans. Ind. Electron.*, vol. 62, no. 1, pp. 310–321, Jan. 2015.

[19] J. Z. Zhou, H. Ding, S. Fan, Y. Zhang, and A. M. Gole, "Impact of short-circuit ratio and phase-locked-loop parameters on the small-signal behavior of a VSC-HVDC converter," *IEEE Trans. Power Del.*, vol. 29, no. 5, pp. 2287–2296, Oct. 2014.

[20] Y. Wang, C. Guo, and C. Zhao, "A novel supplementary frequency-based dual damping control for VSC-HVDC system under weak AC grid," *Int. J. Electr. Power Energy Syst.*, vol. 103, pp. 212–223, Dec. 2018.

[21] A. El Magri, F. Giri, G. Besançon, A. El Fadili, L. Dugard, and F. Z. Chaoui, "Sensorless adaptive output feedback control of wind energy systems with PMS generators," *Control Eng. Pract.*, vol. 21, no. 4, pp. 530–543, Apr. 2013.

[22] A. Watil, A. El Magri, A. Raihani, R. Lajouad, and F. Giri, "Multi-objective output feedback control strategy for a variable speed wind energy conversion system," *Int. J. Electr. Power Energy Syst.*, vol. 121, Oct. 2020, Art. no. 106081.

[23] B. Yang, Y. Y. Sang, K. Shi, W. Yao, L. Jiang, and T. Yu, "Design and real-time implementation of perturbation observer based sliding-mode control for VSC-HVDC systems," *Control Eng. Pract.*, vol. 56, pp. 13–26, Nov. 2016.

[24] W. Wang, X. Yin, L. Jiang, Y. Cao, and Y. Li, "Perturbation observer-based nonlinear control of VSC-MTDC systems," *Int. J. Electr. Power Energy Syst.*, vol. 134, Jan. 2022, Art. no. 107387.

[25] I. E. Myasse, A. E. Magri, M. Kissaoui, R. Lajouad, A. Watil, and C. Berrahal, "Adaptive nonlinear control of generator load VSC-HVDC association," *IFAC-PapersOnLine*, vol. 55, no. 12, pp. 782–787, 2022.

[26] K. El Mezdi, A. El Magri, A. Watil, I. El Myasse, L. Bahatti, R. Lajouad, and H. Ouabi, "Nonlinear control design and stability analysis of hybrid grid-connected photovoltaic-battery energy storage system with ANN-MPPT method," *J. Energy Storage*, vol. 72, Nov. 2023, Art. no. 108747.

[27] J. Beerten, S. D'Arco, and J. A. Suul, "Frequency-dependent cable modelling for small-signal stability analysis of VSC-HVDC systems," *IET Gener., Transmiss. Distrib.*, vol. 10, no. 6, pp. 1370–1381, Apr. 2016.

[28] G. Pinares and M. Bongiorno, "Modeling and analysis of VSC-based HVDC systems for DC network stability studies," *IEEE Trans. Power Del.*, vol. 31, no. 2, pp. 848–856, Apr. 2016.

[29] J. D. Glover, T. J. Overbye, and M. S. Sarma, *Power System Analysis & Design*, 6th ed. Boston, MA, USA: Cengage Learning, 2017.

[30] A. Mansouri, A. El Magri, I. El Myasse, R. Lajouad, and N. Elaadouli, "Backstepping nonlinear control of a five-phase PMSG aerogenerator linked to a Vienna rectifier," *Indonesian J. Electr. Eng. Comput. Sci.*, vol. 32, no. 2, p. 734, Nov. 2023.
[31] H. Hammouri and M. Farza, "Nonlinear observers for locally uniformly observable systems," *ESAIM, Control, Optim. Calculus Variat.*, vol. 9, pp. 353–370, Mar. 2003.
[32] M. Farza, M. M'Saad, and L. Rossignol, "Observer design for a class of MIMO nonlinear systems," *Automatica*, vol. 40, no. 1, pp. 135–143, Jan. 2004.

ILYASS EL MAYSSE (Student Member, IEEE) received the master's degree in control, industrial computer, signals, and systems from Cadi Ayyad University, Marrakesh, Morocco, in 2020. He is currently pursuing the Ph.D. degree in automatic control, transmission energy, and power converters with the Hassan II University of Casablanca, Morocco. His research interests include adaptive control, nonlinear control, and observer design, with applications in power systems and renewable energy conversion systems.

ABDELMOUNIME EL MAGRI received the degree in electrical engineering from ENSET, Rabat, Morocco, in 2001, and the Ph.D. degree in electrical and control engineering from Mohammed V University, Rabat, in 2011. He is currently a Professor with the Higher Normal School of Technical Education, Hassan II University of Casablanca, Morocco. His research interests include nonlinear system identification, nonlinear control, adaptive control, power, and energy systems control.

AZIZ WATIL received the Ph.D. degree in electrical engineering and automatic from the Hassan II University of Casablanca, Morocco, in 2022. His research interests include modeling of dynamical systems, optimization, nonlinear control, and observer design for many applications, including electric power systems, renewable energy conversion systems, and electric vehicles.

ABDULAZIZ ALKUHAYLI received the M.S. degree in electrical engineering from the Missouri University of Science and Technology, Rolla, MO, USA, in 2013, and the Ph.D. degree in electrical engineering from North Carolina State University, Raleigh, NC, USA, in 2018. From 2006 to 2009, he was an Operation Engineer with the Energy Control Center, Saudi Electricity Company. He is currently an Assistant Professor with the Department of Electrical Engineering, King Saud University, Riyadh, Saudi Arabia. His research interests include energy management, renewable energy systems, flexible ac transmission systems, power system stability, and smart grids.

MOHAMMED KISSAOUI received the Ph.D. degree in electrical engineering from Mohammed V University, Rabat, Morocco, in 2016. He is currently a Professor with the Hassan II University of Casablanca, Morocco. His research interests include optimization, observation, and nonlinear control of uninterruptible power supplies and active power filters. He has coauthored several papers on these topics.

RACHID LAJOUAD was born in 1974. He received the Ph.D. degree in electrical engineering from Mohammed V University, Rabat, Morocco, in 2016. He is currently a Professor with the Hassan II University of Casablanca, Morocco. His research interests include optimization, observation, and nonlinear control of ac machines and renewable energy. He has published several journal/conference papers on these topics.

FOUAD GIRI received the Ph.D. degree in automatic control from the Institut National Polytechnique de Grenoble, Grenoble, France, in 1988. He is currently a Professor with the University of Caen Normandie, France. His research interests include non-linear system identification, observation and control, and application to power electric systems. He has published more than 300 journal/conference papers.

MOHAMED METWALLY MAHMOUD was born in Sohag, Egypt. He received the B.Sc., M.Sc., and Ph.D. degrees in electrical engineering from Aswan University, Egypt, in 2015, 2019, and 2022, respectively. He is currently a Professor with Aswan University. His research interests include performance improvement of wind generators, optimization methods, intelligent controllers, fault ride-through capability, power quality, FACTS tools, and energy storage systems. He has been awarded Aswan University prizes for international publishing, in 2020, 2021, and 2022, respectively.